

Inductive and Electrostatic Acceleration in Relativistic Jet-Plasma Interactions

Johnny S. T. Ng and Robert J. Noble

Stanford Linear Accelerator Center, Stanford University, Stanford, CA 94309

We report on the observation of rapid particle acceleration in numerical simulations of relativistic jet-plasma interactions and discuss the underlying mechanisms. The dynamics of a charge-neutral, narrow, electron-positron jet propagating through an unmagnetized electron-ion plasma was investigated using a three-dimensional, electromagnetic, particle-in-cell computer code. The interaction excited magnetic filamentation as well as electrostatic plasma instabilities. In some cases, the inductively generated longitudinal electric fields reached the relativistic plasma wave-breaking limit, and the longitudinal momentum of about half the positrons increased by 50% with a maximum gain exceeding a factor of two.

Relativistic outflows are commonly observed in astrophysical sources such as active galactic nuclei and micro-quasars. Their interaction with ambient plasma is believed to give rise to particle acceleration producing the observed radiation spectrum ranging from radio to gamma-ray. Acceleration occurs when the galactic nucleus' energy carried by the outflow is transferred to the surrounding material. In some models, the mechanism relies on the stochastic scattering of particles among the magnetic fields created by magnetohydrodynamic shocks. Alternatively, jet kinetic energy could be converted into plasma instabilities which in turn power particle acceleration and nonthermal radiation. The microphysical details are complex. The subject is an area of active research and has been reviewed elsewhere [1, 2].

In this Letter, we report on the observation of particle acceleration in simulation studies of relativistic jet-plasma interactions, and elucidate the relevant physical mechanisms. We explore the evolution of narrow, charge-neutral, electron-positron jets propagating through a stationary, unmagnetized electron-ion plasma. This geometry allows us to explore both the plasma microphysics occurring in the jet core and at the jet-plasma boundary, in the limit of no background magnetic field. By studying this simple jet-plasma system, our work sheds light on fundamental questions regarding the processes by which jet-plasma interactions cause particle acceleration. These results are applicable to narrow jets of micro-quasars or the interface region of wide jets (or other relativistic outflows) in contact with an ambient background plasma.

When charge-neutral plasmas stream through each other it is well-known that filamentation occurs via a process commonly referred to as Weibel instability [3]. Essentially, the Lorentz force associated with magnetic field perturbations due to local current imbalances causes the moving neutral plasma to charge-separate transversely, and the resulting current filaments strengthen

the azimuthal magnetic field perturbation in a positive feed-back mechanism. The result is that a neutral jet quickly breaks up into oppositely charged filaments. Filament size is on the order of a collision-less skin depth $\lambda_p = c/\omega_{pe}$, where c is the speed of light, and $\omega_{pe} = \sqrt{4\pi e^2 n_e/m_e}$ is the electron plasma frequency, e the electron charge, n_e the plasma electron density and m_e the electron mass. Filamentary structures have been observed in various plasma systems ranging from solar flares, extragalactic jets [4, 5, 6], and laboratory electron beams [7].

Particle-in-cell (PIC) simulation is well-suited to study these complex phenomenon. In this technique, the motion of an assembly of charged particles is followed in their self-consistent electric and magnetic fields, and the solutions to the equation of motion and Maxwell's equations are determined numerically on discrete spatial coordinates [8, 9]. In practice, the number of particles followed is limited and each particle can be viewed as representing many particles in a real plasma (a macro-particle).

Recent PIC simulation studies of filamentation in astrophysical plasmas have concentrated on wide jets using periodic boundary conditions to study the interior dynamics [10, 11, 12, 13]. Astrophysical observations have indicated instabilities might also be taking place at the boundary region of the jet, at the interface of the flowing relativistic plasma and surrounding material. It was the goal of this work to simulate the interaction of a relativistic jet several λ_p wide so that the dynamics in the core as well as at the jet-plasma boundary can be investigated. We study finite length as well as continuously flowing jets.

Our PIC code is based on the TRISTAN [14] package modified for our particular simulation setup. TRISTAN is a three-dimensional, electromagnetic, relativistic particle-in-cell code employing a so-called local elec-

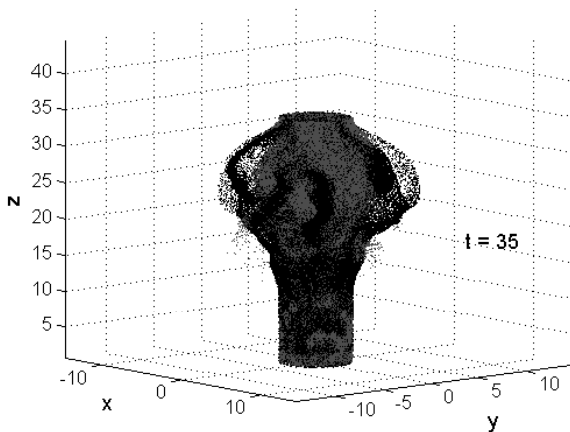


FIG. 1: Spatial distribution of electrons (gray dots) and positrons (black dots) of a continuous jet. Background plasma is not shown. The coordinates are in units of λ_p , and t is in units of ω_{pe}^{-1} .

tromagnetic field solver without the need for transform methods [15]. The temporal and spatial scales are normalized to ω_{pe}^{-1} and λ_p of the background plasma, respectively. The electromagnetic fields are normalized to the relativistic plasma-wave breaking value $E_{pw} = m_e c \omega_{pe} / e$. Each simulation run thus represents a family of cases with arbitrary background plasma density because this parameter has been scaled out. The jet's relativistic factor γ , diameter, length, and the jet-plasma density ratio, as well as the time-step size and the number of macro-particles per cell can all be set independently.

Figure 1 illustrates our simulation geometry and shows a $6 \lambda_p$ wide continuous jet at a simulation time step of $t = 35 \omega_{pe}^{-1}$. The jet enters at the bottom of the simulation box and travels along the z direction, with initial $\gamma = 10$ and spread $\Delta\gamma/\gamma = 0.1\%$. The cold electron plasma fills the entire box uniformly. The ratio of jet to plasma density is 10. The values of γ and the density ratio were chosen for convenience such that the jet's Weibel growth rate would be approximately equal to the background plasma frequency. The micro-physics presented here occur within a duration of $45 \omega_{pe}^{-1}$. For a typical background plasma density of 0.01 cm^{-3} , ω_{pe}^{-1} corresponds to a millisecond. A time-step size of $0.1 \omega_{pe}^{-1}$ was adequate to resolve this physics, as confirmed by runs with $0.05 \omega_{pe}^{-1}$ time-steps. For a Courant parameter of 0.5, this corresponded to a mesh size of $0.2 \lambda_p$.

Simulations were performed on a $150 \times 150 \times 225$ grid with a total of about 40 million macro-particles. In units of λ_p , the box size was 30×30 transversely ($x \times y$) and 45 longitudinally (in z). The TRISTAN boundary conditions were set such that radiation at the box walls was absorbed to simulate free space with no reflections. Particles leaving the box were lost from the simulation, al-

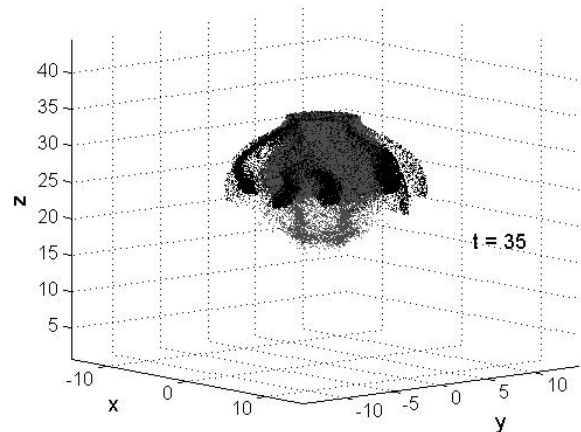


FIG. 2: Spatial distribution of electrons (gray dots) and positrons (black dots) of a $10 \lambda_p$ long jet. Background plasma is not shown. The coordinates are in units of λ_p , and t is in units of ω_{pe}^{-1} .

though we recorded the energy they carried away. Typically the simulation box was made large enough so that few jet particles ever leave during the entire simulation and less than 0.5% of the jet energy was carried away. We varied our simulation parameters, and found that our results were not sensitive to the box size, nor the number of macro-particles per cell once this number was in the range of 4 to 8.

Continuous and finite length jets occur in nature. Figure 2 illustrates our simulation of a $10 \lambda_p$ long jet. Both types exhibit the same transverse dynamics but different longitudinal dynamics.

As expected for the Weibel instability, the electromagnetic energy grows exponentially and then saturates at approximately 10% of the initial jet energy. The growth rate in the laboratory frame is approximately $\omega_{pj}/\sqrt{\gamma}$ [16], where $\omega_{pj} = \sqrt{4\pi e^2 n_j / m_e}$ is the jet's plasma frequency, n_j being the jet density. The jet filament size is on the order of c/ω_{pj} . Our simulations confirm the scaling with n_j and γ . At $t \sim 20 \omega_{pe}^{-1}$ the instability has saturated for our parameters. As the jet continues to plow forward, the Lorentz force between the electron and positron filaments tend to push them apart. The electron filaments, however, are confined by the electrostatic channel formed by the heavier-mass ($m_i = 192 m_e$) background plasma ions. The positron filaments are preferentially expelled from the core of the jet. In Figure 2, approximately 50% of the positrons have left the jet's initial radial boundary.

As the positron filaments move away from the core and from each other, the azimuthal magnetic field (B_ϕ) associated with the filaments decrease rapidly. According to Faraday's law of induction, the time-variation of magnetic flux generates a loop-integrated electric field enclos-

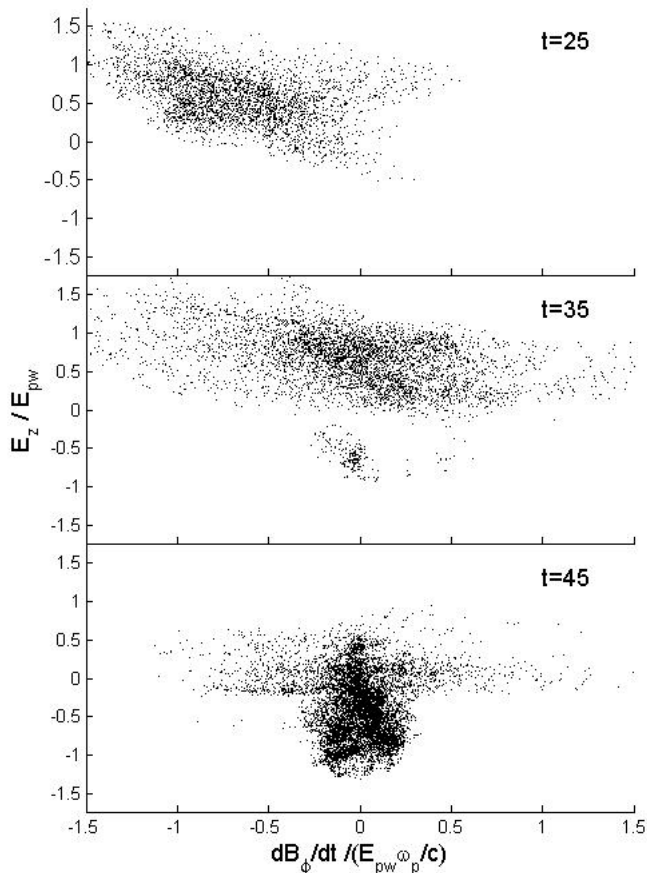


FIG. 3: Correlation of longitudinal electric field with time variation of azimuthal magnetic field, in normalized units, is shown for a $10 \lambda_p$ long jet. For clarity, only fields outside a radius of $2.5 \lambda_p$ are shown.

ing the flux region. In our simulation, we find that this large and negative \dot{B}_ϕ locally induces a large and positive longitudinal electric field E_z . The correlation between E_z and \dot{B}_ϕ , at the same spatial location, is shown in Figure 3 at three epochs of the simulation.

This inductively generated E_z field propagates at the same subluminal velocity as the filaments, and continues until the filaments are fully separated at $t \sim 45 \omega_{pe}^{-1}$. In the continuous jet case, E_z persists throughout the simulation duration as more energy is injected along with the jet. Based on experience with terrestrial accelerators, this E_z can efficiently accelerate particles as they “surf” on a slow wave of electric fields in the direction of motion. In this case, it preferentially accelerates comoving positrons and decelerates electrons.

For the finite-length jet case, a second field generating mechanism develops as the positron filaments are expelled, leaving behind the electron filaments in the jet core. Our investigation of this configuration was motivated by the observation of density variations along the length of some astrophysical jets, due to either a longi-

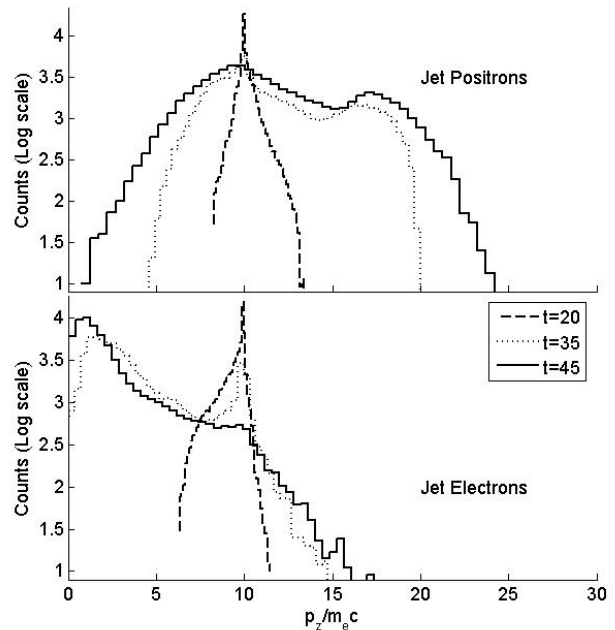


FIG. 4: Longitudinal momentum distribution of positrons and electrons at three simulation epochs for a $10 \lambda_p$ long jet. Time t is in units of ω_{pe}^{-1} .

tudinal plasma instability or the pulsed nature of the source. We found that starting at about $30 \omega_{pe}^{-1}$ for our parameters, a coherent train of electrostatic plasma waves was excited behind the electron jet analogous to the wake of a ship in water. These waves are evident in Figure 3 at $t = 35 \omega_{pe}^{-1}$, with the development of a bipolar E_z field at $\dot{B}_\phi = 0$. They are unlike the inductive shock already discussed, having no associated transverse magnetic field over their interior volume, and only limited surface magnetic fields at their extreme edges, as expected for a finite-size plasma wave.

These plasma wakefields have a phase velocity equal to the speed of the drive jet, and have amplitudes of order the relativistic wave-breaking limit. We observe that plasma wakes always form immediately behind the trailing edge of the electron jet, regardless of its length. These waves continue to oscillate after the drive jet passes, and hence can accelerate relativistic particles over very long distances [17, 18].

The longitudinal momentum (p_z) distributions of jet positrons and electrons are shown in Figure 4. The positrons gained energy steadily, with approximately 40% of the initial population increasing at least 50% in p_z . Proportionally, the electrons lost energy due to deceleration in the E_z fields. The transverse momentum of the jet particles broadened significantly from the initial distribution, with large gains and losses. This acceleration took place over a period of tens of milliseconds,

which is extremely short on the astronomical scale.

Some of the initial jet energy is also converted into heating the background plasma. The thermal energy of plasma electrons increased to approximately $m_e c^2$. The lighter plasma electrons are expelled by the jet electron filaments as well as entrained by the expanding positron filaments. They leave the jet region quickly, leaving behind a depleted region.

We conclude that an inductive “Faraday acceleration” mechanism can effectively power cosmic particles, and that electrostatic plasma wakefields are excited by an initially charge-neutral, finite-length jet when oppositely charged filaments separate. These are promising directions for further research. So far our computation has been limited by the capabilities of typical personal computers. The jet-plasma interaction should be followed for a much longer time to study the effect of plasma wakefield acceleration. The effect of background magnetic fields should be investigated, as well as other particle mixtures of jet compositions. Furthermore, synchrotron radiation can be readily implemented in a particle-in-cell code and the resulting spectrum can be verified against observation.

Jet-plasma dynamics might also be studied in a terrestrial laboratory environment in order to verify simulations and gain further insights [19]. A neutral “jet” approximately one λ_p wide can be created by combining accelerator electron and positron beams. Alternatively, a partially-charged “jet” several λ_p wide can be created by showering an electron or photon beam in a thick material. The work presented here provides the basis for the design of these experiments.

We appreciate discussions with K.-I. Nishikawa, K. Reil, A. Spitkovsky, and M. Watson. We would also like to thank P. Chen, R. Ruth, and R. Siemann for their

support and encouragement. Work supported by the U.S. Department of Energy under contract number DE-AC02-76SF00515.

-
- [1] R. D. Blandford, *Astrophys. J. Supp. Ser.* **90**, 515 (1994).
 - [2] J. G. Kirk, in *Proc. 22nd Texas Symp. on Rel. Astrophys.*, edited by P. Chen *et al.* (2005), SLAC-R-752.
 - [3] E. S. Weibel, *Phys. Rev. Lett.* **2**, 83 (1959).
 - [4] R. A. Perley *et al.*, *Astroph. J.* **285**, L35 (1984).
 - [5] F. N. Owen *et al.*, *Astroph. J.* **340**, 698 (1989).
 - [6] A. P. Lobanov and J. A. Zensus, *Science* **294**, 128 (2001).
 - [7] M. Tatarakis *et al.*, *Phys. Rev. Lett.* **90**, 175001 (2003).
 - [8] J. Dawson, *Rev. Mod. Phys.* **55**, 403 (1983).
 - [9] C. K. Birdsall and A. B. Langdon, *Plasma Physics via Computer Simulation* (IOP Publishing Ltd., Bristol, England, 1991).
 - [10] L. O. Silva *et al.*, *Astrophys. J.* **596**, L121 (2003).
 - [11] J. T. Frederiksen *et al.*, *Astrophys. J.* **608**, L13 (2004).
 - [12] C. B. Hededal *et al.*, *Astrophys. J.* **617**, L107 (2004).
 - [13] K. I. Nishikawa *et al.*, *Astrophys. J.* **622**, 927 (2005).
 - [14] O. Buneman, in *Computer Space Plasma Physics: Simulation Techniques and Software*, edited by H. Matsumoto and Y. Omura (Terra Scientific Publishing, Tokyo, Japan, 1993).
 - [15] J. Villasenor and O. Buneman, *Comp. Phys. Comm.* **69**, 306 (1992).
 - [16] P. Yoon and R. C. Davidson, *Phys. Rev. A* **35**, 2718 (1987).
 - [17] T. Tajima and J. M. Dawson, *Phys. Rev. Lett.* **43**, 267 (1979).
 - [18] P. Chen *et al.*, *Phys. Rev. Lett.* **54**, 693 (1985).
 - [19] J. S. T. Ng, in *Proc. 28th ICFE Advanced Beam Dynamics Workshop* (Higashi Hiroshima, Japan, 2003), SLAC-PUB-10134.